No. 2
ISSN 0809–4403 Sept. 2010

Semi-analytical large displacement analysis of stiffened imperfect plates with a free or stiffened edge

by

Lars Brubak and Jostein Hellesland

E - PRINT SERIES
MECHANICS AND APPLIED MATHEMATICS

UNIVERSITY OF OSLO
DEPARTMENT OF MATHEMATICS
MECHANICS DIVISION

UNIVERSITETET I OSLO
MATEMATISK INSTITUTT
AVDELING FOR MEKANIKK

Dept. of Math., University of Oslo
Mechanics and Applied Mathematics,
E - print Series No. 2
ISSN 0809–4403 Sept. 2010

Semi-analytical large displacement analysis of stiffened imperfect plates with a free or stiffened edge

Lars Brubak and Jostein Hellesland

Mechanics Division, Department of Mathematics,
University of Oslo, NO-0316 Oslo, Norway

Abstract

A large deflection, semi-analytical method is developed for pre- and postbuckling analyses of stiffened rectangular plates with one edge free or flexibly supported, and the other three edges laterally supported. The plates can have stiffeners in both directions parallel and perpendicular to the free edge, and the stiffener spacing can be arbitrary. Both global and local bending modes are captured by using a displacement field consisting of displacements representing a simply supported, stiffened plate and an unstiffened plate with a free edge. The out-of-plane and in-plane displacements are represented by trigonometric functions and linearly varying functions, defined over the entire plate. The formulations derived are implemented into a FORTRAN computer programme, and numerical results are compared with results by finite element analyses (FEA) for a variety of plate and stiffener geometries. Relatively high numerical accuracy is achieved with low computational efforts.

Key words:
Stiffened plates; Free edge; Semi-analytical method; Large deflection theory; Local–global bending interaction; Buckling; Postbuckling; Rayleigh-Ritz method

Notation

b	Plate width (in y-direction)
D	$= Et^3/12(1-\nu^2)$ Plate stiffness
d_i	Displacement amplitudes
E	Young's modulus
f_Y	Yield strength

L	Plate length (in x-direction)
S_x	External stress (positive in compression)
t	Plate thickness
u	In-plane displacements (x-direction)
u_i^a, u_{ij}^b, u^c	Displacement amplitudes
v	In-plane displacements (y-direction)
v_i^a,v_{ij}^b, v^c	Displacement amplitudes
w	Out-of-plane displacements (z-direction)
w_i^a, w_{ij}^b	Displacement amplitudes
w_0	Model imperfection
$w_{,x}$	$= \partial w/\partial x$
$w_{,xy}$	$= \partial^2 w/\partial x \partial y$
ν	Poisson's ratio
σ_x, σ_y	In-plane stresses (positive in tension)
τ_{xy}	In-plane shear stress

1 INTRODUCTION

Semi-analytical analysis methods for buckling and postbuckling behaviour and strength of plates are quite common, in particular in computer based design codes [1, 2]. These methods are usually tailor-made approaches for specific cases with certain boundary conditions and load conditions, and they are not so general as finite element analyses (FEA). This will increase the computational efficiency as compared to a more general problem description, but on the other hand, restrict the range of applicability.

In the present study, axially compressed rectangular plates with a free or a stiffened edge are of interest. For such plates, most of the semi-analytical methods available are considering the elastic buckling (eigenvalue) characteristics of unstiffened plates, e.g. [3, 4, 5, 6, 7, 8]. In the present research work, the main focus is on postbuckling analysis of the plate response, in which the displacements and stresses are predicted.

The major objective is to develop a semi-analytical, large deflection (nonlinear) theory model for analysis of imperfect, unstiffened or stiffened rectangular plates, laterally supported at three edges and with one edge being free or provided with an edge stiffener. The proposed model is based on an incremental form of the Rayleigh-Ritz method and it is able to trace the pre- and postbuckling response including the plate stresses. The plate stresses can subsequently be used in combination with suitable strength criteria in order to predict approximate ultimate strengths. However, such strength estimates are outside the scope of the present paper.

The model is able to capture the interaction between local and global plate bending, and it is able to trace the pre- and postbuckling response including asymmetric effects. The adopted stiffener modelling is simplified and is not capable of predicting local failure modes of the stiffeners, which, consequently, must be designed such that they do not buckle prematurely.

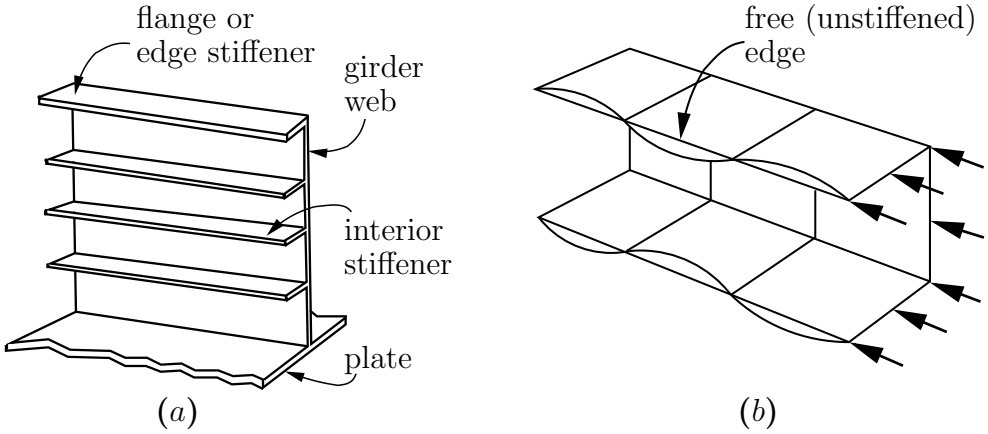

Figure 1. (a) Section of a typical stiffened girder with an edge provided with a stiffener, and (b) a free edge example of a flange outstand of a channel beam.

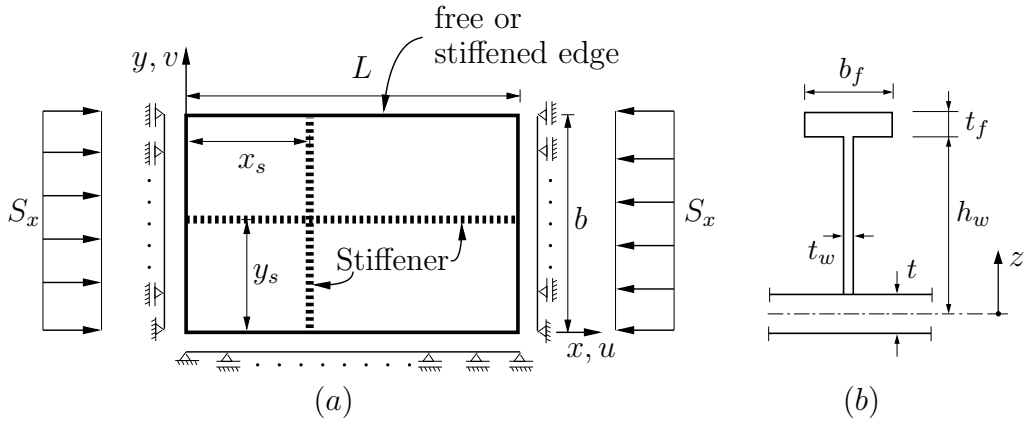

Figure 2. (a) A uniaxially loaded, stiffened plate with a free edge and three continuously supported edges and (b) an eccentric stiffener.

2 PROBLEM FORMULATION AND PLATE DEFINITION

In many branches, such as marine, bridge and aerospace engineering, plated structures with stiffened plates are used as main load-carrying components. A plated structure may consist of both integrated plates (i.e. plates surrounded by neighbouring plates and strong girders at all edges) and plates with a free or stiffened edge. Longitudinal and transverse girders, and stringer decks in a ship structure, are examples where the web plates can have a completely free edge or an edge provided with a flange or an edge stiffener as illustrated in Fig. 1(a). In addition, the interior plating of such girder webs can be provided with horizontal stiffeners, as shown in the figure, or vertical stiffeners. Another example is the channel section with flange outstands illustrated in Fig. 1(b).

The rectangular plate considered can be defined with reference to Fig. 2. Three edges are supported (continuously) in the out-of-plane direction, and the last

edge is either completely free or provided with an edge stiffener. Two opposite supported edges, perpendicular to the free or stiffened edge, are subjected to an external stress S_x. The plate interior may be unstiffened, or it may be stiffened with one or more stiffeners oriented in the x- and y-direction. In Fig. 2(a), only one stiffener is shown in each direction. However, none or multiple stiffeners may be included. The spacing between the stiffeners can be arbitrarily chosen. The stiffeners may have different cross-section profiles, and may be eccentric, as in Fig. 2(b), or symmetric about the middle plane of the plate. The stiffeners may be end loaded (continuous stiffeners) or sniped at the ends (with no end loads).

A plate is usually a part of a larger structure and it is assumed that the supported edges remain straight due to neighbouring plates. In addition, the loaded edges are free to move in the in-plane directions, but they are forced to remain parallel. A supported edge boundary may be simply supported, or it may be clamped or partially restrained by adding rotational spring restraints along the edges, or parts of the edges, in the same manner as described in Brubak and Hellesland [9].

The stiffeners are modelled as simple beams, and consequently, lateral deflections of the stiffeners are not accounted for. With this assumption, the stiffeners must be dimensioned such that premature local stiffener buckling does not occur. This can be done for instance by satisfying constructional design requirements in existing design rules, e.g., [10, 11], which are given to prevent local failure modes of the stiffeners. By using such design rules, the compressive stresses in the stiffeners will not exceed the critical stress for local stiffener buckling. Consequently, in such cases, the present stiffener modelling approach, neglecting local buckling of the stiffeners, seems reasonable.

The St. Venant torsional stiffness of the stiffeners may be accounted for by including the corresponding torsional energy contribution. This contribution is neglected for the cases studied in this paper, where only open stiffener profiles are considered, such as for instance T-profiles and flat bar profiles. This neglect is reasonable as the torsional stiffness of stiffeners with such profiles is relatively small. In addition, it is conservative to neglect this contribution. On the other hand, for stiffeners with closed profiles, the torsional stiffness may be large and it may be too conservative to neglect this stiffness contribution.

3 DISPLACEMENT FIELD

3.1 Previous studies

The accuracy and convergence of the semi-analytical method depend on the selection of displacement fields. Many researchers have studied different admissible displacement functions for plates with an unsupported edge. A usual assumption for such cases is to use a trigonometric series in the direction parallel to the free edge combined with polynomial functions in the perpendicular direction.

In a recent eigenvalue analysis work by Mittelstedt [3], various displacement functions in the direction perpendicular to the free edge were studied, including various polynomial functions and a term with a cosine function. In that work, it was found that an ordinary polynomial function was the most appropriate

displacement function. The same conclusion was also drawn in eigenvalue studies by Smith, Bradford and Oehlers [4], where both ordinary and orthogonal polynomials were studied. In that paper, it was found that orthogonal polynomials were computationally more expensive than simple, ordinary polynomials, despite a reduced number of terms required for adequate convergence. Ordinary polynomials have also been applied in many other works on eigenvalue analysis, e.g., in Madhavan and Davidson [5, 6], Qiao and Shan [7], and Yu and Schafer [8]. All the semi-analytical methods for plates with free edges mentioned above are restricted to linear elastic buckling (eigenvalue) of unstiffened plates.

3.2 Present displacement field

For postbuckling analysis of thin plates, a usual approach is to describe the problem by out-of-plane displacements only. Then, the in-plane stresses and strains must be found by solving the plate compatibility equation [12]. In previously presented semi-analytical methods for simply supported plates [13, 14], this equation have been solved by substituting an assumed Airy's stress function. For unstiffened plates with a free edge, a solution for the Airy's stress function is found by Ovesy, Loughlan and Assaee [15] using a finite strip approach. However, for semi-analytical approaches using a displacement field defined over the entire plate, it is difficult, and maybe impossible, to find an analytical expression for the Airy's stress function that satisfies both the plate compatibility equation and the boundary conditions for a plate with a free edge.

Another approach is to use an assumed displacement field for each displacement component u, v and w. It is this approach that is presented in this paper. By introducing assumed displacements also in the in-plane directions, more degrees of freedom are needed and a larger system of equations must be solved, which affects the computation time. However, an advantage of including in-plane displacements is that the difficulty of solving the plate compatibility equation for a stiffened plate with a free edge is avoided, and the stress computations becomes much more efficient. Once all the displacements (u, v, w) are known, the internal stresses and strains can be computed directly from Hooke's law.

The chosen displacement field in each direction consists of a field representing an unstiffened plate with a free edge, identified by a super index 'a', and a simply supported (along all edges), stiffened plate, identified by a super index 'b'. These displacement fields also account for the in-plane stress redistribution due to out-of-plane bending. In addition, a linear in-plane displacement field, identified by a super index 'c', is added to the displacement field in the x- and y-direction in order to account for linear variations. The displacement fields are given by

$$w = w^a + w^b \tag{1}$$

$$u = u^a + u^b + u^c \tag{2}$$

$$v = v^a + v^b + v^c \tag{3}$$

Here, the out-of-plane w-displacements (z-direction) are defined by

$$w^a(x,y) = \sum_{i=1}^{M_{wa}} w_i^a \frac{y}{b} \sin(\frac{\pi i x}{L}) \tag{4}$$

$$w^b(x,y) = \sum_{i=1}^{M_{wb}} \sum_{j=1}^{N_{wb}} w_{ij}^b \sin(\frac{\pi i x}{L}) \sin(\frac{\pi j y}{b}) \ , \tag{5}$$

the in-plane u-displacements (x-direction) are defined by

$$u^a(x,y) = \sum_{i=1}^{M_{ua}} u_i^a \frac{y}{b} \sin(\frac{\pi i x}{L}) \tag{6}$$

$$u^b(x,y) = \sum_{i=1}^{M_{ub}} \sum_{j=1}^{N_{ub}} u_{ij}^b \sin(\frac{\pi i x}{L}) \sin(\frac{\pi j y}{b}) \tag{7}$$

$$u^c(x,y) = u^c \frac{x}{L} \ , \tag{8}$$

and the in-plane v-displacements (y-direction) are defined by

$$v^a(x,y) = \sum_{i=1}^{M_{va}} v_i^a \frac{y}{b} \cos(\frac{\pi i x}{L}) \tag{9}$$

$$v^b(x,y) = \sum_{i=1}^{M_{vb}} \sum_{j=1}^{N_{vb}} v_{ij}^b \sin(\frac{\pi i x}{L}) \sin(\frac{\pi j y}{b}) \tag{10}$$

$$v^c(x,y) = v^c \frac{y}{b} \tag{11}$$

where w_i^a, w_{ij}^b, u_i^a, u_{ij}^b, u^c, v_i^a, v_{ij}^b, v^c are amplitudes, L the plate length and b the plate width.

With these displacement fields, the total number of degrees of freedom is

$$N_{\text{dof}} = M_{ua} + (M_{ub} \times N_{ub}) + M_{va} + (M_{vb} \times N_{vb}) + M_{wa} + (M_{wb} \times N_{wb}) + 2 \tag{12}$$

Similar displacement fields to those representing a simply supported plate (Eqs. (5), (7) and (10)), but with only one term in each direction, are used in Bazant [16] to study simply supported, unstiffened plates. By including more terms in the displacement fields in each direction, it is also possible to model stiffened plates in the same manner as in Brubak et al. [14, 9, 17]. For the displacement fields representing a plate with a free edge (Eqs. (4), (6) and (9)), each displacement component consists of a trigonometric series in the x-direction in the same manner as in Ovesy, Loughlan and GhannadPour [18], and a linear variation in y-direction.

3.3 Discussion/comments

Some additional comments of the chosen displacement fields might be in order. As mentioned before, polynomial functions in the y-direction have been used in many eigenvalue studies of plates with a free edge, e.g., Mittelstedt [3], Madhavan and Davidson [5, 6], Qiao and Shan [7], and Yu and Schafer [8]. In these works, unstiffened plates were studied, and for such plates it is not necessary to used

many terms in order to achieve satisfactory results. However, for stiffened plates, this may not be so.

In preliminary stages of the present work, displacements with polynomial functions with many terms were studied. In that study, an eigenvalue problem was established for an assumed displacement field defined by

$$w^{po}(x,y) = \sum_{i=1}^{M_w} \sum_{j=1}^{N_w} w_{ij}^{po} \left(\frac{y}{b}\right)^j \sin(\frac{\pi i x}{L}) \tag{13}$$

where w_{ij}^{po} denotes the displacement amplitudes. In order to describe the displacements for an unstiffened plate, a polynomial with 3 or 4 terms in Eq. (13) will normally be enough. For such few terms, no numerical problems occurred in the test study. However, by using Eq. (13) for a stiffened plate, many terms must be included to describe the displacements. In principle, the more terms that are included in the polynomial function, the more exact the solution becomes. However, numerical tests using the polynomial function showed that numerical problems occur if many polynomial terms are included. As a result of this, it was decided to replace the displacement field in Eq. (13) by the combined displacement field defined by Eq. (4) and (5).

Unlike in Eq. (13), the assumed displacement fields used in the present method (Eqs. (4), (6) and (9)) includes only a linear variation in the y-direction. With this simplification, no numerical problems occurred. The approximation implied by the use of only a linear variation is partly compensated for by adding the trigonometric series representing a simply supported stiffened plate (Eqs. (5), (7) and (10)).

4 MATERIAL LAW AND KINEMATIC RELATIONSHIPS

For thin isotropic plates, the stresses in the thickness direction are negligibly small and it is usual to assume a plane stress condition. Further, for a material that is assumed to be linearly elastic with Young's modulus E and Poisson's ratio ν, the well known Hooke's law applies. It is defined by

$$\sigma_x = \frac{E}{1-\nu^2}(\epsilon_x + \nu\epsilon_y)\,; \quad \sigma_y = \frac{E}{1-\nu^2}(\epsilon_y + \nu\epsilon_x) \tag{14}$$

$$\tau_{xy} = \frac{E}{2(1+\nu)}\gamma_{xy} = G\gamma_{xy} \tag{15}$$

where σ_x, σ_y and τ_{xy} are the in-plane stresses, and ϵ_x, ϵ_y and γ_{xy} the in-plane strains, defined positive in tension. The total strain at a distance z from the middle plane of the plate can be written as

$$\epsilon_x = \epsilon_x^{pm} - z w_{,xx}\,; \qquad \epsilon_y = \epsilon_y^{pm} - z w_{,yy} \tag{16}$$

$$\gamma_{xy} = \gamma_{xy}^{pm} - 2z w_{,xy} \tag{17}$$

where the first terms, with the super index 'pm', represent the membrane strains and the second terms expressed by out-of-plane displacements w are the bending strains. These out-of-plane displacements w are additional to an initial imperfection. The conventional "comma" notation is used for partial

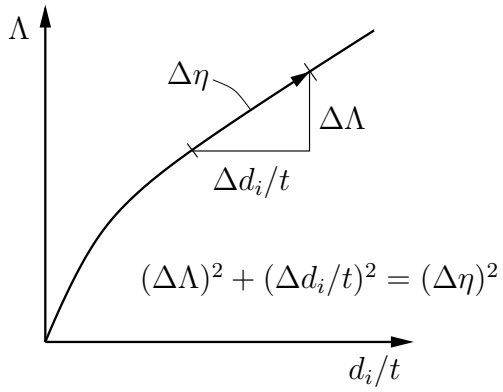

Figure 3. Illustration of the relationship between $\Delta\eta$, a load increment $\Delta\Lambda$ and an increment in the displacements for a case with one amplitude d_i.

differentiation, i.e., $w_{,xy}$ for $\partial^2 w/\partial x\partial y$, etc. The bending strain distribution complies with Kirchhoff's assumption [19] that normals to the middle plane remain normal to the deflected middle plane. For the membrane strains, the classical large deflection theory [16] is used (large rotations, but small in-plane strains). The in-plane membrane strains are defined by

$$\epsilon_x^{pm} = u_{,x} + \frac{1}{2}w_{,x}^2 + w_{0,x}w_{,x} \tag{18}$$

$$\epsilon_y^{pm} = v_{,y} + \frac{1}{2}w_{,y}^2 + w_{0,y}w_{,y} \tag{19}$$

$$\gamma_{xy}^{pm} = u_{,y} + v_{,x} + w_{,x}w_{,y} + w_{0,x}w_{,y} + w_{0,y}w_{,x} \tag{20}$$

for a plate with an initial out-of-plane imperfection w_0. These formulations with w_0 included were given by Marguerre [12] in order to extend the von Karman's plate theory [19] to cases with initial imperfections.

5 SOLUTION PROCEDURE

5.1 Incremental response propagation

The postbuckling response is traced using an incremental procedure presented by Steen [20] and Steen, Byklum and Hellesland [21], in which an arc length parameter is used as a propagation (incrementation) parameter. By using an arc length parameter (η), this procedure is more general than methods with pure load or pure displacement control, and a complex plate response can be handled, including equilibrium curves with snap-through and snap-back. This procedure has been applied in several other research works, in which the out-of-plane displacements were the only assumed displacements, e.g., Byklum and Amdahl [13], Brubak and Hellesland [14], Byklum, Steen and Amdahl [22], and Steen et al. [21]. Also the in-plane displacements are included in the present paper. As a consequence, coupling terms between the in-plane and out-of-plane displacements appear in the equations that describe the plate response. This complicates the expressions in the incremental response propagation.

In the large deflection theory, the equilibrium equations obtained using the Rayleigh-Ritz method are nonlinear in the displacements. In order to avoid solving nonlinear equations directly, the equilibrium equations are solved incrementally by computing the rate form of the equilibrium equations with respect to the arc length parameter η. The change in the arc length parameter can be related directly to a change in the external stresses and displacements. For an external applied stress that is changing proportionally with a load factor parameter Λ, this relation is illustrated graphically in Fig. 3 for the single displacement amplitude. In the limit, as the increment size approaches zero, it can in the general case be expressed as

$$\dot{\Lambda}^2 + \sum_{i=1}^{N_{\text{dof}}} \frac{\dot{d}_i^2}{t^2} = 1 \tag{21}$$

Here, a dot above a symbol ($\dot{\Lambda}$, etc.) means differentiation with respect to the arc length parameter η, which can be considered a pseudo-time. Further, t is plate thickness introduced in order to obtain dimensional consistency, N_{dof} is the total number of degrees of freedom, d_i represents the elements in a vector consisting of an assembly of all the displacement amplitudes and $\dot{d}_i$ is the corresponding rates. The displacement amplitude vector, defined by the displacement amplitudes, can be written as

$$\begin{aligned}[d_i] =& \left[d_1, d_2, d_3, ..., d_{N_{\text{dof}}} \right] \\ =& \Big[u_1^a, ..., u_{M_{ua}}^a, u_{11}^b, u_{12}^b, ..., u_{M_{ub}N_{ub}}^b, u^c, v_1^a, ..., v_{M_{va}}^a, v_{11}^b, \\ & v_{12}^b, ..., v_{M_{vb}N_{vb}}^b, v^c, w_1^a, ..., w_{M_{va}}^a, w_{11}^b, w_{12}^b, ..., w_{M_{wb}N_{wb}}^b \Big]\end{aligned} \tag{22}$$

where, for instance, $d_1 = u_1^a$ and $d_{N_{\text{dof}}} = w_{M_{wb}N_{wb}}^b$.

The load factor Λ and displacement amplitudes d_i are functions of the arc length parameter η. For an increment $\Delta\eta$ along the equilibrium curve from point "k" to"$k+1$", a Taylor series expansion gives

$$d_i^{k+1} = d_i^k + \dot{d}_i^k \Delta\eta + \frac{1}{2}\ddot{d}_i^k \Delta\eta^2 + ... \tag{23}$$

$$\Lambda^{k+1} = \Lambda^k + \dot{\Lambda}^k \Delta\eta + \frac{1}{2}\ddot{\Lambda}^k \Delta\eta^2 + ... \tag{24}$$

The second and higher order terms are neglected in the present paper, resulting in a first order expansion. The approximation based on only the first order expansion is usually referred to as the Euler or Euler-Cauchy method. In other works, such as in Steen [20] and Byklum [23], it is shown how to include the second order terms. However, in the latter work, it was found that significant computational gains (efficiency) are not achieved by retaining the second order terms as compared to the Euler method with smaller increments.

The accuracy of the present method can also be improved by using equilibrium corrections after each increment, for instance such as in Riks' arc length method [24], or alternatively by using an improved Euler method (Heun's method), which is a predictor-corrector method [25]. However, these improvements are also computationally costly and will not likely result in significant computational gains although they allow for larger increments to be used.

5.2 Incremental stiffness relationship

Equilibrium is satisfied using the principle of stationary potential energy (Rayleigh-Ritz method) on an incremental form (rate form), defined by $\delta\dot{\Pi} = \delta\dot{U} + \delta\dot{T} = 0$, where Π is the total potential energy, U is the strain energy and T is the potential energy of the external loads. This leads to N_{dof} linear equations in $N_{\text{dof}} + 1$ unknowns. Using index notation with the Einstein summation rule for repeated indices, they may be given by

$$\frac{\partial\dot{\Pi}}{\partial d_i} = \frac{\partial}{\partial\eta}\frac{\partial\Pi}{\partial d_i} = K_{ij}\dot{d}_j + G_i\dot{\Lambda} = 0 \ , \qquad i,j = 1,2,...,N_{\text{dof}} \tag{25}$$

where

$$K_{ij} = \frac{\partial^2\Pi}{\partial d_i \partial d_j} \text{ and } G_i = \frac{\partial^2\Pi}{\partial d_i \partial\Lambda} \tag{26}$$

The additional equation required is given by Eq. (21). Above, K_{ij} is a generalised, incremental (tangential) stiffness matrix, $-G_i\dot{\Lambda}$ is a generalised, incremental load vector and d_j is the displacement amplitudes.

Alternatively, in the common matrix notation, the final set of $N_{\text{dof}} + 1$ equations can be given by

$$\mathbf{K}\dot{\mathbf{d}} + \mathbf{G}\dot{\Lambda} = 0 \quad \text{ and } \quad \dot{\Lambda}^2 + \frac{1}{t^2}\dot{\mathbf{d}}^T\dot{\mathbf{d}} = 1 \tag{27}$$

The incremental stiffness matrix, load vector and displacement vector can conveniently be divided into submatrices and subvectors as given by

$$\mathbf{K} = \begin{bmatrix} \mathbf{K}_{uu} & \mathbf{K}_{uv} & \mathbf{K}_{uw} \\ \mathbf{K}_{vu} & \mathbf{K}_{vv} & \mathbf{K}_{vw} \\ \mathbf{K}_{wu} & \mathbf{K}_{wv} & \mathbf{K}_{ww} \end{bmatrix}, \quad \mathbf{G} = \begin{bmatrix} \mathbf{G}_u \\ \mathbf{G}_v \\ \mathbf{G}_w \end{bmatrix}, \quad \mathbf{d} = \begin{bmatrix} \mathbf{u} \\ \mathbf{v} \\ \mathbf{w} \end{bmatrix} \tag{28}$$

Further, for each displacement component (u, v, w), these submatrices and subvectors are subdivided into new submatrices and subvectors corresponding to the displacement assumptions previously labelled with super indices 'a', 'b' and 'c'. The displacements, may then be written

$$\mathbf{u} = \begin{bmatrix} \mathbf{u}_a \\ \mathbf{u}_b \\ \mathbf{u}_c \end{bmatrix} = \left[u_1^a, ..., u_{M_{ua}}^a, u_{11}^b, u_{12}^b, ..., u_{M_{ub}N_{ub}}^b, u^c\right]^T \tag{29}$$

$$\mathbf{v} = \begin{bmatrix} \mathbf{v}_a \\ \mathbf{v}_b \\ \mathbf{v}_c \end{bmatrix} = \left[v_1^a, ..., v_{M_{va}}^a, v_{11}^b, v_{12}^b, ..., v_{M_{vb}N_{vb}}^b, v^c\right]^T \tag{30}$$

$$\mathbf{w} = \begin{bmatrix} \mathbf{w}_a \\ \mathbf{w}_b \end{bmatrix} = \left[w_1^a, ..., w_{M_{wa}}^a, w_{11}^b, w_{12}^b, ..., w_{M_{wb}N_{wb}}^b\right]^T \tag{31}$$

The vectors $-\dot{\Lambda}\mathbf{G}_u$, $-\dot{\Lambda}\mathbf{G}_v$ and $-\dot{\Lambda}\mathbf{G}_w$ are subdivided in a similar manner. All the bold face vectors and subvectors in the expressions above are column vectors. More details of the subdivision of the matrices and vectors are given in Appendix *A*. For complete details, see Brubak [26].

5.3 Procedure for solving the equations

In order to trace the equilibrium curve, the solution of the system of equations must be found. As mentioned above, Eq. (25) represents $N_{\text{dof}} \times N_{\text{dof}}$ linear equations in the $N_{\text{dof}} \times N_{\text{dof}} + 1$ unknowns ($\dot{d}_j$ and $\dot{\Lambda}$) and Eq. (21) is the additional equation required. The solution of Eq. (25) is given by

$$\dot{d}_j = -\dot{\Lambda} K_{ij}^{-1} G_i = \dot{\Lambda} Q_j \quad \text{where } Q_j = -K_{ij}^{-1} G_i \tag{32}$$

By substituting Eq. (32) into Eq. (21), the following equation is obtained

$$\dot{\Lambda}^2 (t^2 + \sum_{j=1}^{N_{\text{dof}}} Q_j^2) = t^2 \tag{33}$$

from which the load rate parameter $\dot{\Lambda}$ can be determined as

$$\dot{\Lambda} = \pm \frac{t}{\sqrt{t^2 + \sum_{j=1}^{N_{\text{dof}}} Q_j^2}} \tag{34}$$

There are two possible solutions with the same numerical value, but with opposite signs. One solution is in the direction of an increasing arc length and one in the opposite direction. The solution of interest corresponds to that giving a continuous increase of the arc length. This is assumed to be the solution which results in the smoothest equilibrium curve. In the same manner as in Steen [20], this is expressed by the requirement that the absolute value of the angle between the tangents of two consecutive states ("$k-1$" and "k") in the load-displacement ($\Lambda - d_j/t$) space is smaller than 90 degrees. Thus, for the correct sign of the load rate $\dot{\Lambda}^k$ at state "k", the following criterion must be satisfied:

$$\sum_{j=1}^{N_{\text{dof}}} \dot{\Lambda}^k \left(\frac{Q_j^k \dot{d}_j^{k-1}}{t^2} + \dot{\Lambda}^{k-1}\right) > 0 \tag{35}$$

An equivalent formulation for choosing the correct sign is given in Byklum et al. [13]. When $\dot{\Lambda}^k$ is found, the corresponding displacement rates $\dot{d}_j^k$ are found by Eq. (32).

6 POTENTIAL ENERGY

6.1 Potential strain energy of the plate

The potential strain energy of the plate gives contribution to the incremental stiffness matrix. Each contribution to the potential energy of the plate is given

below, and the manner it affects the computational time is discussed. Due to large and complex expressions, the rate form of these contributions is not given here, but can be found in Brubak [26].

For thin plates, the potential strain energy U^p can be given by

$$U^p = \frac{1}{2}\int_V \boldsymbol{\sigma}^T \boldsymbol{\epsilon}\, dV \tag{36}$$

where $\boldsymbol{\sigma} = [\sigma_x, \sigma_y, \tau_{xy}]^T$, $\boldsymbol{\epsilon} = [\epsilon_x, \epsilon_y, \gamma_{xy}]^T$ and V is the volume of the plate. It is common to divide the strain energy into a membrane contribution and a bending contribution. Then, Eq. (36) can be written as

$$\begin{aligned} U^p &= \frac{1}{2}\int_V (\boldsymbol{\sigma}^{pm} + \boldsymbol{\sigma}^{pb})^T (\boldsymbol{\epsilon}^{pm} + \boldsymbol{\epsilon}^{pb})\, dV \\ &= \frac{1}{2}\int_V (\boldsymbol{\sigma}^{pm})^T \boldsymbol{\epsilon}^{pm}\, dV + \frac{1}{2}\int_V (\boldsymbol{\sigma}^{pb})^T \boldsymbol{\epsilon}^{pb}\, dV \\ &= U^{pm} + U^{pb} \end{aligned} \tag{37}$$

where the super indices '*pm*' and '*pb*' are used to identify the membrane and the bending contributions, respectively. The coupling terms between the membrane and bending contribution disappear when integrating over the plate thickness, since the bending stresses are zero at the middle plane of the plate and are varying linearly in the thickness direction.

Potential bending strain energy. By substituting Hooke's law into the bending part of Eq. (37) and then integrating this contribution over the plate thickness, the elastic strain energy contribution from bending of the plate can be written as [19]

$$U^{pb} = \frac{D}{2}\int_0^b \int_0^L \left((w_{,xx} + w_{,yy})^2 - 2(1-\nu)(w_{,xx}w_{,yy} - w_{,xy}^2) \right) dx\, dy \tag{38}$$

where $D = Et^3/12(1-\nu^2)$ is the plate bending stiffness and t the plate thickness. By substituting the assumed displacement field, an analytical solution of this integral may be derived. This energy contribution is of quadratic order in the displacement amplitudes. Thereby, it gives a constant contribution to the incremental plate stiffness matrix since this matrix is obtained by differentiation twice with respect to the displacement amplitudes (Eq. (26)). Consequently, it is necessary to computed this matrix only once. The bending stiffness matrix of the plate on rate form can be found in Brubak [26].

Potential membrane strain energy. By substituting Hooke's law into the membrane part of Eq.(37), the elastic membrane strain energy of the plate can be written as [19]

$$U^{pm} = \frac{C}{2}\int_0^b \int_0^L \left((\epsilon_x^{pm})^2 + (\epsilon_x^{pm})^2 - 2\nu(\epsilon_x^{pm})(\epsilon_y^{pm}) - \frac{1-\nu}{2}(\gamma_{xy}^{pm})^2 \right) dx\, dy \tag{39}$$

where $C = Et/(1-\nu^2)$ is the extensional stiffness of the plate. By substituting the membrane strains from Eqs. (18)-(20) and the assumed displacement fields into this equation, an analytical solution of this integral may be derived. The resulting expression can be separated into a term U^{pmL} that is quadratic in the

displacement amplitudes and a term U^{pmNL} that is of a higher order in the amplitudes. The membrane strain energy can then be written as

$$U^{pm} = U^{pmL} + U^{pmNL} \tag{40}$$

The first term in Eq. (40), differentiated twice with respect to the amplitudes, gives a constant contribution, labelled $\mathbf{K}^{pmL}$, to the total incremental stiffness matrix in Eq. (27), or in Eq. (26). Thus, this matrix must be calculated only once, and does not affect the computation time significantly. Similarly, the second term in Eq. (40) provides a nonlinear contribution, labelled $\mathbf{K}^{pmNL}$, to the incremental stiffness matrix. This latter matrix is dependent on the displacement amplitudes, and consequently it must be calculated for every increment in the solution propagation described in Section 5. Thus, this matrix affects the computational efficiency significantly.

6.2 Potential energy of external plate loads

The potential energy of the external stresses contribute to the incremental load vector $-\dot{\Lambda}\mathbf{G}$. The potential energy of an external, in-plane load acting on the plate in the x-direction is given by

$$T^{p,x} = -\Lambda S_{x0} t b \Delta u \tag{41}$$

where S_{x0} is a reference stress (positive in compression as shown in Fig. 2), $\Delta u = u^c$ is the plate shortening in the x-direction and Λ is the load factor. An analytical expression of $-\dot{\Lambda}\mathbf{G}$ is given in Brubak [26].

The potential energy of an external lateral pressure acting on the plate in the z-direction can be given by

$$T^{p,z} = -\int_0^b \int_0^L p\, w \, dx \, dy \tag{42}$$

where $p = p(x, y)$ is the lateral pressure. This contribution gives a constant contribution to the incremental load vector. This load case is not included in the present paper.

6.3 Potential energy of stiffeners

The potential energy of the stiffeners consists of a strain energy contribution and an energy contribution due to external stiffener loads, which give contributions to the incremental stiffness matrix and the incremental load vector, respectively.

Potential strain energy of a stiffener parallel to the free edge. The elastic strain energy of the stiffener is given by [14, 27]

$$\begin{aligned} U^{s,x} =& \frac{E}{2} \int_0^L \int_{A_s} \epsilon_x^2 \, dA_s dx \\ =& \frac{EI}{2} \int_0^L z^2 w_{,xx}^2 \, dx - e_c E A_s \int_0^L \epsilon_x^{pm} w_{,xx} \, dx + \frac{E A_s}{2} \int_0^L (\epsilon_x^{pm})^2 \, dx \end{aligned} \tag{43}$$

where I is the moment of inertia (second moment of area) of the stiffener about $z = 0$ (at the midplane of the plate), A_s is the stiffener cross-section area and e_c is the distance from the middle plane of the plate to the centre of area of the stiffener. The integrand in Eq. (43), must be evaluated at the stiffener location $y = y_s$ defined in Fig. 2. By substituting the strain ϵ_x^{pm} from Eq. (18) and the assumed displacement field into Eq. (43), an analytical solution can be derived. In a similar manner as for the membrane strain energy of the plate, the strain energy of the stiffener can be separated into a term that is quadratic in the displacement amplitude and a term of a higher order. Then, $U^{s,x}$ can be written as

$$U^{s,x} = U^{sL,x} + U^{sNL,x} \tag{44}$$

where $U^{sL,x}$ and $U^{sNL,x}$ give a linear contribution, labelled $\mathbf{K}^{sL,x}$, and a nonlinear contribution, labelled $\mathbf{K}^{sNL,x}$, to the incremental stiffness matrix, respectively. These two matrices can be found in Brubak [26].

The torsional stiffness of the stiffeners may be accounted for in a simplified manner by including the St. Venant torsion energy contribution given by

$$U^{sT,x} = \frac{GJ}{2} \int_0^L w_{,xy}^2 dx \tag{45}$$

where J is the torsion constant and $G = E/2(1 + \nu)$. The integrand must be evaluated at the stiffener location $y = y_s$. This contribution may be significant in conjunction with torsionally stiff, closed stiffener profiles. In the open stiffener profile examples of the present paper, the torsional stiffener stiffness is neglected. This is normally acceptable for such profiles. The strain energy due to torsion of a stiffener is quadratic in the displacement amplitudes. It will therefore give a contribution only to the linear incremental stiffness matrix $\mathbf{K}^{sL,x}$.

Potential strain energy of a stiffener perpendicular to the free edge. The elastic strain energy of the stiffener is given by

$$\begin{aligned} U^{s,y} =& \frac{E}{2} \int_0^b \int_{A_s} \epsilon_y^2 \, dA_s dy \\ =& \frac{EI}{2} \int_0^b z^2 w_{,yy}^2 \, dy - e_c E A_s \int_0^b \epsilon_y^{pm} w_{,yy} \, dy + \frac{EA_s}{2} \int_0^b (\epsilon_y^{pm})^2 \, dy \end{aligned} \tag{46}$$

In similar manner to the stiffener parallel to the free edge, the integrand must be evaluated at the stiffener location $x = x_s$ defined in Fig. 2. Further, this contribution can also be separated into a term that is quadratic and a term of a higher order. Then, $U^{s,y}$ can be written as

$$U^{s,y} = U^{sL,y} + U^{sNL,y} \tag{47}$$

where $U^{sL,y}$ and $U^{sNL,y}$ give a linear contribution, labelled $\mathbf{K}^{sL,y}$, and a nonlinear contribution, labelled $\mathbf{K}^{sNL,y}$, to the incremental stiffness matrix, respectively. Details of these two matrices can be found in Brubak [26].

The St. Venant torsional stiffness of the stiffeners may again be accounted by including the energy contribution given by

$$U^{sT,y} = \frac{GJ}{2} \int_0^b w_{,xy}^2 dy \tag{48}$$

The integrand must be evaluated at the stiffener location $x = x_s$.

Potential energy of external stiffener loads in the x-direction The stiffeners may be end loaded (typical for continuous stiffeners) if the stiffener ends are attached to a surrounding structure. For a continuous longitudinal stiffener parallel to the free edge, the potential energy of the external loads can be taken according to

$$T^{s,x} = -P_{sx}\Delta u - P_{sx}e_c w_{2,x} + P_{sx}e_c w_{1,x} \tag{49}$$

where P_{sx} is the resultant force (positive in compression) of stresses acting on the stiffener. In this expression, $w_{1,x}$ and $w_{2,x}$ are the rotations of the stiffener end located at $x = 0$ and $x = L$, respectively. The two last terms in Eq. (49) are contributions due to the rotation of the stiffener about the y-axis at the stiffener ends. This expression is similar to an expression for potential energy of external stiffener loads previously given by Brubak and Hellesland [14], and by Steen [27] for a stiffened plate with only one degree of freedom. In the present paper, end loaded stiffeners are not considered.

7 VERIFICATION PREMISES

For verification of the present semi-analytical model, a variety of plate and stiffener dimensions have been considered. Computed results by the present model have been compared with linearly elastic, geometric nonlinear finite element analyses (FEA, using either ANSYS [28] or ABAQUS [29]) in which both plate and stiffeners were modelled using shell elements. The finite element model is supported in the out-of-plane direction along three edges and it has one edge being free or provided with an edge stiffener. In the same manner as for the proposed model, the plate is subjected to an external axial stress at the two opposite, supported edges, perpendicular to the free edge. The supported edges are forced to remain straight during deformation, and further, the loaded edges remain parallel. The plate is also supported in the in-plane directions, just enough to prevent rigid body motions. In the cases studied, the ends of the stiffeners are completely free and they are not subjected to any external loads.

In the presented results, the number of degrees of freedom used in the FEA for a stiffened plate is typically about 15000, which is a sufficiently large number to ensure satisfactory results. A typical element mesh is shown later (Fig. 10(b)). Probably, sufficient accuracy could have been obtained with fewer degrees of freedom.

In comparison, the number of degrees of freedom is about 260 in the proposed semi-analytical model for all the cases studied. The chosen number of terms in each displacement field is

$$\begin{aligned} &M_{wa} = 1, \quad M_{wb} = N_{wb} = 6, \\ &M_{ua} = M_{ub} = N_{ub} = M_{va} = M_{vb} = N_{vb} = 10 \end{aligned} \tag{50}$$

in all cases, except the snap-back case (Section 9) in which $M_{wa} = 3$.

The present load-deflection results are computed without accounting for material yielding, and the response curves are arbitrarily terminated when the external stress S_x reaches the yield stress $f_Y = 235$ MPa. The adopted elastic

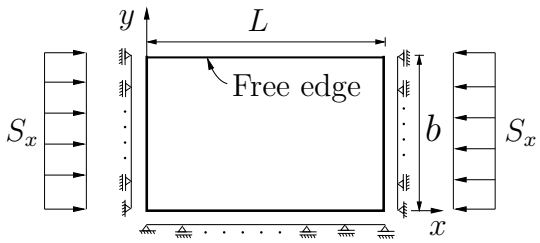

	L	b	t
Plate 1	1000	1000	12
Plate 2	2000	1000	30

Figure 4. Overview and dimensions [mm] of unstiffened plates with a free edge.

material properties in each computation are Young's modulus $E = 208000$ MPa and Poisson's ratio $\nu = 0.3$.

The imperfection shape in the model and the FEA is taken equal to the first eigenmode of the plate as calculated by the respective methods. Details of a simplified eigenmode and elastic buckling stress limit (ESL) calculation used in conjunction with the proposed method are given in Brubak [26]. For verification purposes, the specified maximum amplitude is taken equal to $w_{0,\text{spec}} = 5$mm both in the proposed model and the FEA.

In addition to the chosen number of degrees of freedom, also the incremental step size $\Delta\eta$, will affect the computation time. In the present comparisons with FEA results, a value of $\Delta\eta = 0.04$ is used if not noted otherwise. This is a rather small value and has been found to be satisfactory in previous investigations [14].

8 LOAD-DISPLACEMENT RESULTS

8.1 Unstiffened plates with a free edge

Two typical unstiffened plates with three simply supported edges and one free edge are analysed. These plates, as defined in Fig. 4, have intermediate to relatively large slenderness values in order to study cases with rather nonlinear load-displacements curves. These plates represent relatively severe test cases for the present model.

The displacement shapes of the plates computed by FEA (using ANSYS) and by the present model are very similar. This can be seen in Fig. 5(a) and (b), in which the additional out-of-plane displacements fields w are plotted for Plate 1 subjected to an external stress $S_x = f_y$. Similar comparisons have also been made of the in-plane displacement fields in the x- and y-direction. Again, the results, not included in the present paper, are very similar to each other.

In Figs. 6-7, response curves are shown in which the external stress S_x is plotted both versus the end shortening Δ_x (a) and versus the additional out-of-plane displacement w_{me} at the midlength of the free edge (b). The results are given in a non-dimensional form. In the figures, t is the plate thickness, f_Y

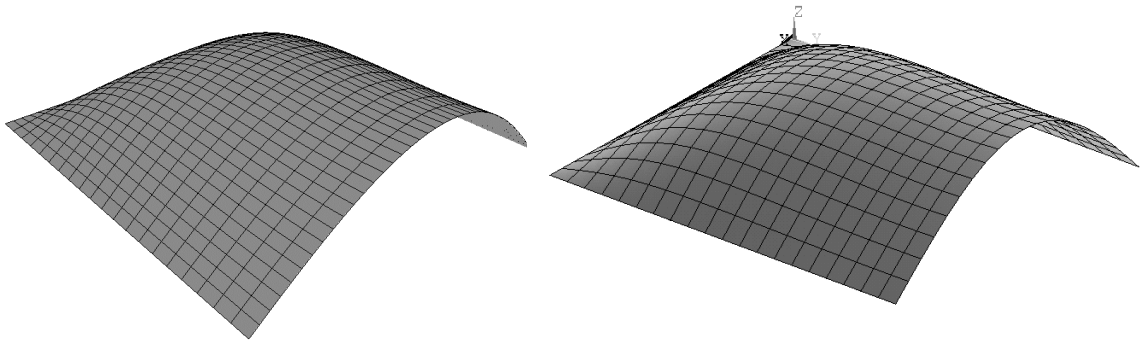

(a) (b)

Figure 5. The bending mode of Plate 1 subjected to an external load $S_x = f_Y$ computed (a) by the present model and (b) by FEA.

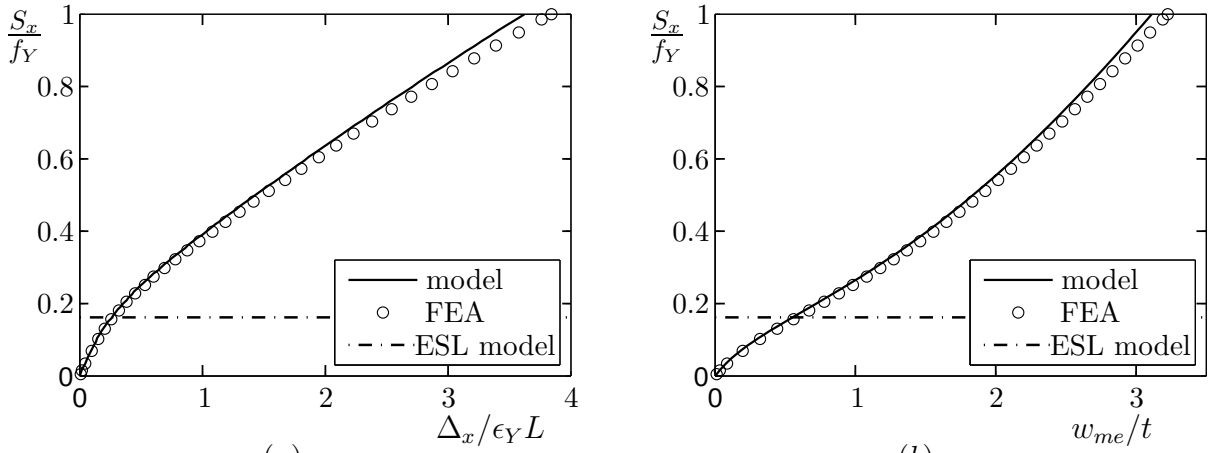

(a) (b)

Figure 6. (a) Load-shortening and (b) load-deflection curves of Plate 1 (slender plate) subjected to a uniaxial load S_x.

the yield stress and $\epsilon_Y = f_Y/E$ $(= 0.00113)$ is the yield strain. The agreement between the response curves computed by the present model (thick solid curves) and by FEA (open dots) is good. It can be seen that the curves obtained by the present model is slightly to the non-conservative side. By increasing the number of terms (degrees of freedom) in the displacement fields, the agreement will improve slightly. However, the present discrepancy is considered to be acceptable.

The end shortening Δ_x (reduction of the distance between two opposite edges) can be considered a "global displacement", while the out-of-plane displacement w_{me} is a "local displacement" at the midlength of the free edge. Consequently, it is expected that the agreement between the present model and the FEA results generally will be better for the load-shortening curves than for the load-deflection curves. This will especially be true for stiffened plates.

The relative elastic buckling stress (eigenvalue) limit (ESL) computed by the present model is also included in the figures (the horizontal dash-dotted

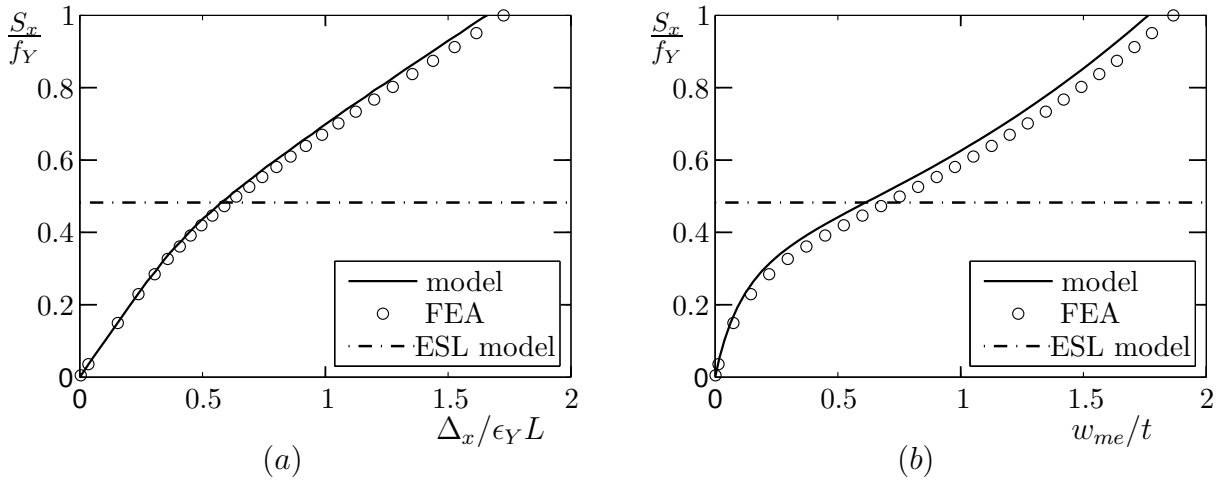

Figure 7. (a) Load-shortening and (b) load-deflection curves of Plate 2 (slender plate) subjected to a uniaxial load S_x.

lines). This stress level (S_x/f_Y) gives an indication of the plate slenderness. The corresponding first eigenmode computed by the FEA and by the present model is quite similar, and as mentioned before, this mode is used as the imperfection shape.

The in-plane stiffness (slope of the load-shortening curve) is significantly reduced when the external stress approaches the elastic buckling stress limit (ESL). This response, as seen in Fig. 6(a) and Fig. 7(a), is expected. With a very small imperfection, the in-plane response will almost be bilinear.

The out-of-plane stiffness (slope of the load-deflection curve), on the other hand, reaches a minimum at load levels close to the ESL, as seen in Fig. 6(b) and Fig. 7(b), and then increases with increasing loads. This behaviour is due to nonlinear membrane effects, and is typical for plates at large out-of-plane displacements.

8.2 Plates with two regular stiffeners and a stiffened edge

Similar results to those presented for the unstiffened plates with a free edge have been obtained for plates with an edge stiffener and two regular interior stiffeners. The three stiffeners are identical and their profiles are eccentric flat bars. An overview of the plate and dimensions are given in Fig. 8.

Also for these plates, the bending modes of the plates computed by the FEA (ANSYS) and by the present model are very similar. A typical case of a global bending mode is shown in Fig. 9(a) and (b), in which the additional out-of-plane displacements w are plotted for Plate 3 subjected to an external stress $S_x = f_y$. In this case, the stiffeners are not strong enough to prevent large plate deflections along the stiffeners. In Fig. 10(a) and (b), similar plots are shown for Plate 4. It can be seen that the bending mode in this case, is a combination of a global and a local bending mode. For Plates 3 and 4, the load-shortening curves are presented in Fig. 11. The agreement between the present model and the FEA results is seen to be good.

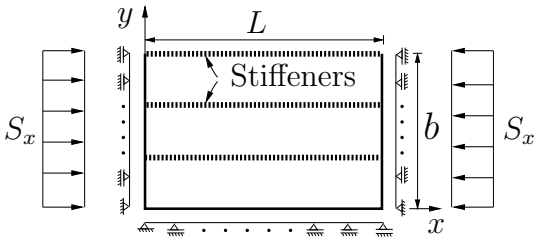

	L	b	t	h_w	t_w
Plate 3	1000	1000	12	56	10
Plate 4	1000	1000	12	106	10

Figure 8. Overview and dimensions [mm] of plates with a stiffened edge and two interior eccentric, flat bar stiffeners.

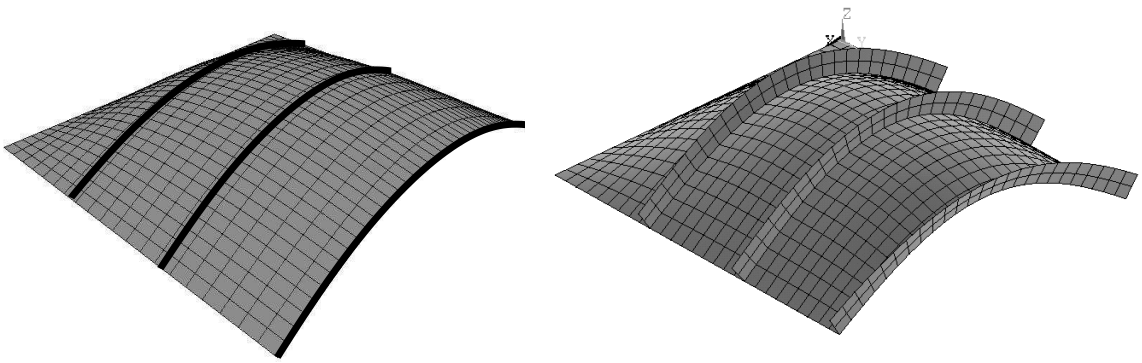

(a) (b)

Figure 9. The bending mode (predominantly global) of Plate 3 subjected to an external load $S_x = f_Y$ computed (a) by the present model and (b) by FEA.

9 SNAP-BACK RESPONSE EXAMPLE

The present semi-analytical method is capable of tracing complex response curves including snap-back and snap-through response curves. This is demonstrated here by an example for an unstiffened plate with length $L = 3000$ mm, breadth $b = 1000$ mm and thickness $t = 14$ mm. The imperfection shape, equal to the first eigenmode of the plate, has one half-wave in the x-direction (parallel to the free edge) and a maximum imperfection of 5 mm at the midlength of the free edge. This example has also been analysed by Andersen [30].

Initially, the deflection shape will be similar to the imperfection shape ("one half wave"). At some load stage, the deflection shape will change into several half waves, and thereby causing a snap-back. In order to be able to capture such snap-back or snap-through responses, it is necessary to include more than one term in the displacement field w^a in Eq. (4). The value of $M_{wa} = 1$ in Eq. (50) is for the present case replaced by $M_{wa} = 3$. This allows a deflection shape with three

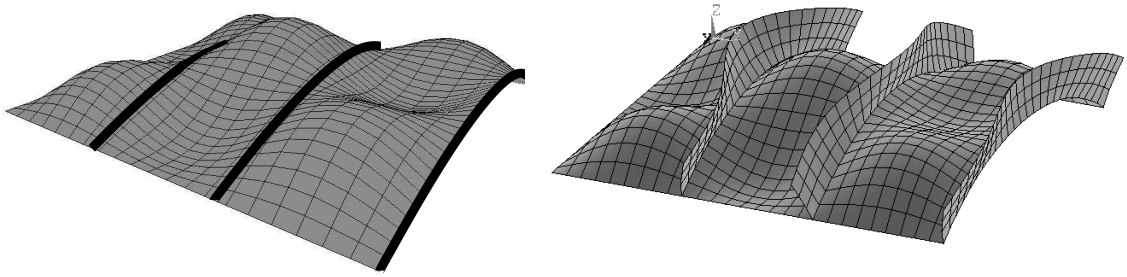

(a) (b)

Figure 10. The bending mode (combined global and local) of Plate 4 subjected to an external load $S_x = f_Y$ computed (a) by the present model and (b) by FEA.

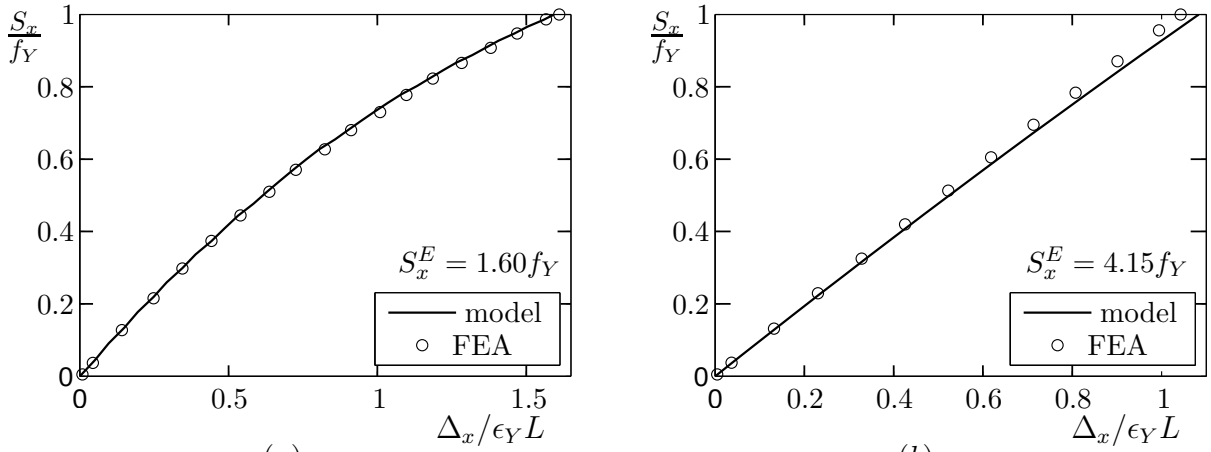

Figure 11. Load-shortening of (a) Plate 3 and (b) Plate 4 subjected to a uniaxial load S_x.

half waves in the x-direction, which is sufficient in the present snap-back example.

The load-shortening response computed by the present model (using a very small arc length increment of $\Delta\eta = 0.005$) and by the FEA (by ABAQUS) is presented in Fig. 12. The agreement between the curves is very good. It can been seen that the response is very unstable, and at a certain load level, both the load and the plate shortening decrease. This is characteristic for a snap-back equilibrium curve.

The deflection shape before and after the snap-back are shown in Fig. 13. It can be seen that the deflection shape has changed from one half wave to three half waves in the x-direction. This was expected, and it was the reason for choosing $M_{wa} = 3$.

It should be noted that a snap-back response occurs very late in the post-buckling region, and it is therefore of more academic than practical interest. The intention was to demonstrate that such complex responses are well captured

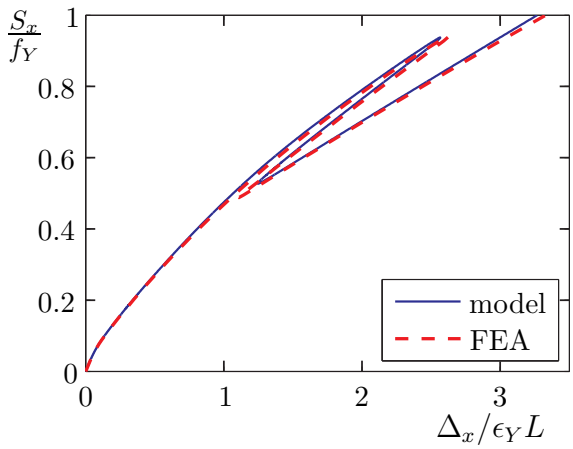

Figure 12. A snap-back load-shortening response computed by the semi-analytical model and FEA.

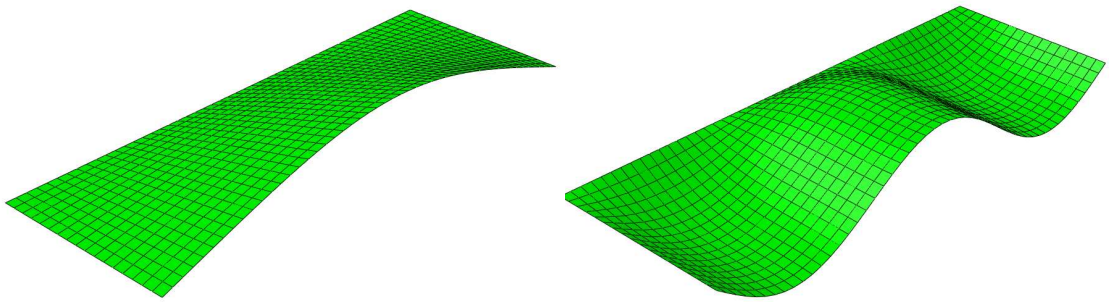

(a) (b)

Figure 13. Deflection shape (a) before and (b) after snap-back of an unstiffened plate with a free edge and three simply supported edges.

by the present solution procedure. Usually, if material yielding is accounted for, the ultimate strength is reached before snapping occurs. Typically, ultimate strength is reached when the plate shortening Δ_x is about $\epsilon_Y L$ (or $\Delta_x/\epsilon_Y L \approx 1$). In comparison, for this case, snapping occurs at a plate shortening Δ_x about $2.5\,\epsilon_Y L$.

10 CONCLUDING REMARKS

An efficient computational model is presented for large deflection postbuckling analysis of imperfect, stiffened rectangular plates with an edge being free or provided with an edge stiffener. The applicability of the present method is documented for several cases, including snap-back problems, by comparison with finite element analysis results. The model is able to trace the plate response beyond the elastic buckling load. It is able to capture both local and global

displacement modes as well as the asymmetric global bending behaviour of plates with eccentric stiffeners. Due to the computational efficiency of the model, it is also suited for design optimisation and reliability studies that normally require a large number of case studies.

ACKNOWLEDGEMENTS

The authors would like to thank dr. scient. Eivind Steen at Det Norske Veritas (DNV) for his interest, suggestions and valuable discussions during the study.

REFERENCES

[1] E. Steen and E. Byklum and K.G. Vilming and T.K. Østvold, Computerized buckling models for ultimate strength assessments of stiffened ship hull panels, Proceedings of The Ninth International Symposium on Practical Design of Ships and other Floating Structures, Lübeck-Travemünde, Germany, Sept. 12-17, 2004; 235–242

[2] J.K. Paik, ALPS/ULSAP user's manual, Ship Structural Mechanics Lab., Department of Naval Architecture and Ocean Engineering, Pusan National University, Busan, Korea, 2003

[3] C. Mittelstedt. Stability behaviour of arbitrarily laminated composite plates with free and elastically restrained unloaded edges, International Journal of Mechanical Sciences, 2007; 49(7): 819–833

[4] S.T. Smith, M.A. Bradford and D.J. Oehlers. Numerical convergence of simple and orthogonal polynomials for the unilateral plate buckling problem using the Rayleigh-Ritz method, International Journal for Numerical Methods in Engineering, 1999; 44(11): 1685–1707

[5] M. Madhavan and J.S. Davidson. Elastic buckling of I-beam flanges subjected to a linearly varying stress distribution, Journal of Constructional Steel Research, 2007; 63(10): 1373–1383

[6] M. Madhavan and J.S. Davidson. Buckling of centerline-stiffened plates subjected to uniaxial eccentric compression, Thin-Walled Structures, 2008; 43(5): 1264–1276

[7] P. Qiao and L. Shan. Explicit local buckling analysis and design of fiber-reinforced plastic composite structural shapes, Composite Structures, 2005; 70(4): 468–483

[8] C. Yu and B.W. Schafer. Effect of longitudinal stress gradients on elastic buckling of thin plates, Journal of Engineering Mechanics, ASCE, 2007; 133(4): 452–463

[9] L. Brubak, J. Hellesland and E. Steen. Semi-analytical buckling strength analysis of plates with arbitrary stiffener arrangements, Journal of Constructional Steel Research, 2007; 63(4): 532–543

[10] EN 1993-1-1, Eurocode 3: Design of steel structures. Part 1.1: General rules and rules for buildings, CEN, European Committee for Standardisation, Brussels, 2005

[11] Det Norske Veritas. Recommended practice DNV-RP-C201, Buckling strength of plated structures, Høvik, Norway, 2002
[12] K. Marguerre. Zur theorie der gekrümmten platte grosser formänderung, Proceedings of The 5^{th} International Congress for Applied Mechanics, 1938; 93–101
[13] E. Byklum and J. Amdahl. A simplified method for elastic large deflection analysis of plates and stiffened panels due to local buckling, Thin-Walled Structures, 2000; 40(11): 925–953
[14] Lars Brubak and Jostein Hellesland. Semi-analytical postbuckling and strength analysis of arbitrarily stiffened plates in local and global bending, Thin-Walled Structures, 2007; 45(6), 620–633
[15] H.R. Ovesy, J. Loughlan, H. Assaee. The compressive post-local bucking behaviour of thin plates using a semi-energy finite strip approach, Thin-Walled Structures, 2004; 42(3): 449–474
[16] Z.P. Bažant and L. Cedolin. Stability of structures, Oxford University Press, 1991
[17] Lars Brubak and Jostein Hellesland. Approximate buckling strength analysis of arbitrarily stiffened, stepped plates, Engineering Structures, 2007; 29(9): 2321–2333
[18] H.R. Ovesy, J. Loughlan, S.A.M. GhannadPour. Geometric non-linear analysis of channel sections under end shortening, using different versions of the finite strip method Computers and Structures, 2006; 84(13-14): 855–872
[19] D.O. Brush and B.O. Almroth. Buckling of bars, plates and shells, McGraw-Hill Book Company, 1975
[20] E. Steen. Application of the perturbation method to plate buckling problems, Research Report in Mechanics, No. 98-1, Mechanics Division, Dept. of Mathematics, University of Oslo, Norway, 1998, 60 pp.
[21] E. Steen, E. Byklum and J. Hellesland. Elastic postbuckling stiffness of biaxially compressed rectangular plates, Engineering Structures, 2008; 30(10): 2631–2643
[22] E. Byklum, E. Steen and J. Amdahl. A semi-analytical model for global buckling and postbuckling analysis of stiffened panels, Thin-Walled Structures, 2004; 42(5): 701–717
[23] E. Byklum. Ultimate strength analysis of stiffened steel and aluminium panels using semi-analytical methods, Dr. ing. thesis, Norwegian University of Science and Technology (NTNU), Trondheim, Norway, 2002
[24] E. Riks. An incremental approach to the solution of snapping and buckling problems, International Journal of Solids and Structures, 1979; 15: 529–551
[25] E. Kreyszig. Advanced Engineering Mathematics, 7th ed., John Wiley & Sons, Inc., 1993
[26] L. Brubak. Semi-analytical postbuckling analysis of stiffened plates with a free edge, Research report in mechanics, No. 08-3, Mechanics Division, Dept. of Mathematics, University of Oslo, Norway, 2008, 98 pp. (can be downloaded from the homepage of department)
[27] E. Steen. Elastic buckling and postbuckling of eccentrically stiffened plates, International Journal of Solids and Structures, 1989; 25(7): 751–768
[28] ANSYS Inc., ANSYS Documentation 11.0, Southpointe, Canonsburg, PA, 2007.
[29] Dassault Systèmes Simulia Corp., ABAQUS Version 6.9 Documentation,

Dassault Systèmes, Providence, RI, USA, 2009.
[30] H.S Andersen, Semi-analytical buckling code development of stiffened and unstiffened plates with a free edge, M.Sc. thesis, Mechanics Division, Department of Mathematics, University of Oslo, Norway, 2010, 111 pp.

A Subdivision of matrices and vectors

In the solution procedure outlined in Section 5, the incremental stiffness matrix $\mathbf{K}$ in Eq. (27) must be computed. For each displacement component (u, v, w), this matrix is divided into submatrices, and it can be written

$$\mathbf{K} = \begin{bmatrix} \mathbf{K}_{uu} & \mathbf{K}_{uv} & \mathbf{K}_{uw} \\ \mathbf{K}_{vu} & \mathbf{K}_{vv} & \mathbf{K}_{vw} \\ \mathbf{K}_{wu} & \mathbf{K}_{wv} & \mathbf{K}_{ww} \end{bmatrix} \tag{A.1}$$

Further, the submatrices ($\mathbf{K}_{uu}$, $\mathbf{K}_{uv}$, etc.) are subdivided into new submatrices corresponding to the displacement assumptions previously labelled with super indices 'a', 'b' and 'c', and they can be written as

$$\mathbf{K}_{uu} = \begin{bmatrix} \mathbf{K}_{uaua} & \mathbf{K}_{uaub} & \mathbf{K}_{uauc} \\ \mathbf{K}_{ubua} & \mathbf{K}_{ubub} & \mathbf{K}_{ubuc} \\ \mathbf{K}_{ucua} & \mathbf{K}_{ucub} & \mathbf{K}_{ucuc} \end{bmatrix}, \quad \mathbf{K}_{vv} = \begin{bmatrix} \mathbf{K}_{vava} & \mathbf{K}_{vavb} & \mathbf{K}_{vavc} \\ \mathbf{K}_{vbva} & \mathbf{K}_{vbvb} & \mathbf{K}_{vbvc} \\ \mathbf{K}_{vcva} & \mathbf{K}_{vcvb} & \mathbf{K}_{vcvc} \end{bmatrix} \tag{A.2}$$

$$\mathbf{K}_{ww} = \begin{bmatrix} \mathbf{K}_{wawa} & \mathbf{K}_{wawb} \\ \mathbf{K}_{wbwa} & \mathbf{K}_{wbwb} \end{bmatrix}, \quad \mathbf{K}_{uv} = \mathbf{K}_{vu}^T = \begin{bmatrix} \mathbf{K}_{uava} & \mathbf{K}_{uavb} & \mathbf{K}_{uavc} \\ \mathbf{K}_{ubva} & \mathbf{K}_{ubvb} & \mathbf{K}_{ubvc} \\ \mathbf{K}_{ucva} & \mathbf{K}_{ucvb} & \mathbf{K}_{ucvc} \end{bmatrix} \tag{A.3}$$

$$\mathbf{K}_{uw} = \mathbf{K}_{wu}^T = \begin{bmatrix} \mathbf{K}_{uawa} & \mathbf{K}_{uawb} \\ \mathbf{K}_{ubwa} & \mathbf{K}_{ubwb} \\ \mathbf{K}_{ucwa} & \mathbf{K}_{ucwb} \end{bmatrix}, \mathbf{K}_{vw} = \mathbf{K}_{wv}^T = \begin{bmatrix} \mathbf{K}_{vawa} & \mathbf{K}_{vawb} \\ \mathbf{K}_{vbwa} & \mathbf{K}_{vbwb} \\ \mathbf{K}_{vcwa} & \mathbf{K}_{vcwb} \end{bmatrix} \tag{A.4}$$

Regarding subscripts, for instance for the matrix $\mathbf{K}_{uava}$, the two first subscripts (ua) indicate the displacement field u^a (Eq. (6)) and the two last subscripts (va) indicate the displacement field v^a (Eq. (9)), and similarly for the other matrices. These submatrices, $\mathbf{K}_{uaua}$, $\mathbf{K}_{uaub}$, etc., are computed by differentiation of the strain energy contributions, twice with respect to the displacement amplitudes reflected by the indices (Eq. (26)). For instance, the stiffness submatrix $\mathbf{K}_{uava}$ is obtained by the expression

$$\mathbf{K}_{uava} = \frac{\partial^2 U}{\partial u_f^a \partial v_p^a} = \begin{bmatrix} \frac{\partial^2 U}{\partial u_1^a \partial v_1^a} & \cdots & \frac{\partial^2 U}{\partial u_1^a v_{Nva}^a} \\ \vdots & & \vdots \\ \\ \frac{\partial^2 U}{\partial u_{Nua}^a \partial v_1^a} & \cdots & \frac{\partial^2 U}{\partial u_{Nua}^a v_{Nva}^a} \end{bmatrix} \tag{A.5}$$

where U is the strain energy. The size of this matrix is equal to $N_{ua} \times N_{va}$, where N_{ua} and N_{va} are the number of terms in the displacement fields u^a and v^a, respectively. A more detailed overview of composition of the submatrices is given in Appendix B. The expressions for all the submatrices can be found in Brubak [26] (and can be downloaded).

In a similar manner as for the incremental stiffness matrix, the incremental load vector $-\dot{\Lambda}\mathbf{G}$ is divided into subvectors for each displacement component (u, v, w). It can be written as

$$-\dot{\Lambda}\mathbf{G}^T = -\dot{\Lambda}[\mathbf{G}_u^T, \mathbf{G}_v^T, \mathbf{G}_w^T] \tag{A.6}$$

These subvectors are subdivided for each displacement field (with super indices 'a', 'b' and 'c'), and they can be written as

$$-\dot{\Lambda}\mathbf{G}_u^T = -\dot{\Lambda}\left[\,\mathbf{G}_{ua}^T,\, \mathbf{G}_{ub}^T,\, \mathbf{G}_{uc}^T\,\right] \tag{A.7}$$

$$-\dot{\Lambda}{\mathbf{G}_\mathbf{v}}^T = -\dot{\Lambda}\left[\,\mathbf{G}_{va}^T,\, \mathbf{G}_{vb}^T,\, \mathbf{G}_{vc}^T\,\right] \tag{A.8}$$

$$-\dot{\Lambda}{\mathbf{G}_\mathbf{w}}^T = -\dot{\Lambda}\left[\,\mathbf{G}_{wa}^T,\, \mathbf{G}_{wb}^T\,\right] \tag{A.9}$$

The subvectors ($-\dot{\Lambda}\mathbf{G}_{ua}$, $-\dot{\Lambda}\mathbf{G}_{ub}$, etc.) obtained in the subdivision for each displacement field are computed by differentiation of the potential energy of the external loads, with respect to the displacement amplitudes and the load factor (Eq. (26)). For instance, the plate contribution of the subvector $-\dot{\Lambda}\mathbf{G}_{ua}$ for a load applied at the plate edge in x-direction is obtained by the expression

$$-\dot{\Lambda}\mathbf{G}_{ua}^p = -\dot{\Lambda}\frac{\partial^2 T^{p,x}}{\partial u_f^a \partial \Lambda} = -\dot{\Lambda}\begin{bmatrix} \frac{\partial^2 T^{p,x}}{\partial u_1^a \partial \Lambda} \\ \vdots \\ \\ \frac{\partial^2 T^{p,x}}{\partial u_{Nua}^a \partial \Lambda} \end{bmatrix} \tag{A.10}$$

All the subvectors of the incremental load vector of the plate can be found in Brubak [26].

B Composition of submatrices and subvectors

An example of the composition of the submatrices and subvectors is explained below for the matrix $\mathbf{K}_{vawb}^{sL,y}$. The super index sL, y indicates the linear stiffness contribution of a stiffener oriented in the y-direction. In line with Eqs. (25)-(26), this matrix can be defined by the expression

$$\mathbf{K}_{vawb}^{sL,y}\dot{\mathbf{w}}^b = \frac{\partial^2 U^{sL,y}}{\partial v_f^a \partial w_{pq}^b}\dot{w}_{pq}^b \tag{B.1}$$

where $U^{sL,y}$ is a stiffener strain energy contribution that is quadratic in the displacements. The composition of this submatrix represents a difficult example, since the displacement amplitudes for two different displacement fields v^a and w^b

and, in addition, the initial imperfection field w_0^a, are involved. In order to make it easier to distinguish between the indices used for the rows and the columns, the product of the submatrix and the displacement rate subvector is given first. By substituting $U^{sL,y}$ into Eq. $(B.1)$, the product can be written

$$\begin{aligned}\mathbf{K}_{vawb}^{sL,y}\dot{\mathbf{w}}^b =& \frac{\partial^2 U^{sL,y}}{\partial v_f^a \partial w_{pq}^b}\dot{w}_{pq}^b \\ =& \sum_{p=1}^{M_{wb}}\sum_{q=1}^{N_{wb}} e_c E A_s \left(\frac{q\pi}{b}\right)^2 \frac{1}{b} I_q^s \cos(\frac{f\pi}{L}x_s)\sin(\frac{p\pi}{L}x_s)\dot{w}_{pq}^b \\ &+ \sum_{p=1}^{M_{wb}}\sum_{q=1}^{N_{wb}}\sum_{m=1}^{M_{wb}} w_{0mq}^b E A_s \left(\frac{q\pi}{b}\right)^2 \frac{1}{2}\cos(\frac{f\pi}{L}x_s)\sin(\frac{p\pi}{L}x_s)\sin(\frac{m\pi}{L}x_s)\dot{w}_{pq}^b\end{aligned} \tag{B.2}$$

where $f = 1, 2, ..., M_{va}$. This product of the submatrix and the displacement rate subvector is a column vector (with row numbers f). Each element in the vector gives a contribution to the equilibrium equations (Eq. (26).

The submatrix alone can be given by

$$\begin{aligned}\mathbf{K}_{vawb}^{sL,y} =& \frac{\partial^2 U^{sL,y}}{\partial v_f^a \partial w_{pq}^b} \\ =& e_c E A_s \left(\frac{q\pi}{b}\right)^2 \frac{1}{b} I_q^s \cos(\frac{f\pi}{L}x_s)\sin(\frac{p\pi}{L}x_s) \\ &+ \sum_{m=1}^{M_{wb}} w_{0mq}^b E A_s \left(\frac{q\pi}{b}\right)^2 \frac{1}{2}\cos(\frac{f\pi}{L}x_s)\sin(\frac{p\pi}{L}x_s)\sin(\frac{m\pi}{L}x_s)\end{aligned} \tag{B.3}$$

where 'f' indicates the row number ($f = 1, 2, ..., M_{va}$), and 'p' and 'q' indicate the column number ($[p, q] = [1, 1], [1, 2]..., [M_{wb}, N_{wb}]$). Thus, the total number of rows is M_{va} and the total number of columns is $M_{wb}N_{wb}$, and the size of the matrix is $M_{va} \times M_{wb}N_{wb}$.

All the expressions for the composition of the remaining submatrices and subvectors in Brubak [26] are similar to the example given above.